Computers in Biology and Medicine 180 (2024) 108899

Contents lists available at ScienceDirect

Computers in Biology and Medicine

journal homepage: www.elsevier.com/locate/compbiomed

A novel ionic model for matured and paced atrial-like human iPSC-CMs integrating I_{Kur} and I_{KCa} currents

Sofia Botti [a,b,*], Chiara Bartolucci [c], Claudia Altomare [e,f,g], Michelangelo Paci [c], Lucio Barile [e,f,g], Rolf Krause [a,d], Luca Franco Pavarino [b], Stefano Severi [c]

[a] Euler Institute, Faculty of Informatics, Università della Svizzera Italiana, Lugano, 6900, Switzerland
[b] Department of Mathematics "Felice Casorati", University of Pavia, Pavia, 27100, Italy
[c] Department of Electrical, Electronic, and Information Engineering "Guglielmo Marconi", University of Bologna, Cesena, 47521, Italy
[d] Faculty of Mathematics and Informatics, UniDistance, Brig, 3900, Switzerland
[e] Cardiovascular Theranostics, Istituto Cardiocentro Ticino, Ente Ospedaliero Cantonale, Lugano, 6900, Switzerland
[f] Laboratories for Translational Research, Ente Ospedaliero Cantonale, Bellinzona, 6500, Switzerland
[g] Euler Institute, Faculty of Biomedical Sciences, Università della Svizzera Italiana, Lugano, 6900, Switzerland

ARTICLE INFO

Keywords:
hiPSC-CMs
Atrial phenotype
Ionic model
Dynamic clamp
Atrial-specific currents
Optimization tools

ABSTRACT

This work introduces the first atrial-specific *in-silico* human induced pluripotent stem cells-derived cardiomyocytes (hiPSC-CMs) model, based on a set of phenotype-specific I_{Kur}, I_{KCa} and I_{K1} membrane currents. This model is built on novel *in-vitro* experimental data recently published by some of the co-authors to simulate the paced action potential of matured atrial-like hiPSC-CMs. The model consists of a system of stiff ordinary differential equations depending on several parameters, which have been tuned by automatic optimization techniques to closely match selected experimental biomarkers. The new model effectively simulates the electronic *in-vitro* hiPSC-CMs maturation process, transitioning from an unstable depolarized membrane diastolic potential to a stable hyperpolarized resting potential, and exhibits spontaneous firing activity in unpaced conditions. Moreover, our model accurately reflects the experimental rate dependence data at different cycle length and demonstrates the expected response to a specific current blocker. This atrial-specific *in-silico* model provides a novel computational tool for electrophysiological studies of cardiac stem cells and their applications to drug evaluation and atrial fibrillation treatment.

1. Introduction

In this study, we propose a novel atrial-like (AL) *in-silico* model of human induced pluripotent stem cells-derived cardiomyocytes (hiPSC-CMs), based on a set of phenotype-specific membrane currents (namely I_{Kur}, I_{KCa} and I_{K1}, defined in Section 2.3). This model is built on novel *in-vitro* experimental data recently published in [1] to simulate the paced action potential (AP) of matured AL hiPSC-CMs.

HiPSC-CMs have greatly advanced the field of Regenerative Medicine since their discovery in 2006 by Yamanaka et al. [2,3], which then led to the Nobel Prize in Medicine in 2012. In the same decade, Yamanaka group refined the capacity to differentiate hiPSCs into disease-relevant cell types such as cardiomyocytes, providing an unprecedented opportunity for the generation of human patient-specific cells for use in disease modelling, personalized drug screening, and regenerative approaches toward precision medicine, see [4–6]. The unlimited production of hiPSC-CMs provides new opportunities to evaluate *in-vitro* models of human cardiomyocytes in normal or pathological conditions that can be used in drug efficacy and safety testing. Moreover, hiPSC-CMs also have the potential to become an essential tool to better understand the familial form of atrial fibrillation (AF), a common disease affecting atrial cells, see [7,8]. The best option currently used for treating the disease is interventional therapy, namely ablation. Several ion channel mutations, along with a range of other genetic variants and broader risk factors, are known to increase the likelihood of developing AF, [9]. Therefore, hiPSC-CMs technology ideally aligns with the patient-specific medicine challenge, since these cells have the same genetic heritage as the donor, [5,10].

In recent years, mathematical models of the hiPSC-CMs ionic currents have focused on immature phenotypes, developing a system of stiff ordinary differential equations (ODEs). Previous studies characterizations of the CMs phenotype were based on AP morphology, but the classification criteria were still undefined. Thus, the forerunner model [11] was based on recordings obtained from a mixture of ventricular-like (VL), atrial-like (AL), and nodal-like hiPSC-CMs and

* Corresponding author at: Euler Institute, Faculty of Informatics, Università della Svizzera Italiana, Lugano, 6900, Switzerland.
E-mail address: sofia.botti@usi.ch (S. Botti).

https://doi.org/10.1016/j.compbiomed.2024.108899
Received 3 May 2024; Received in revised form 25 June 2024; Accepted 14 July 2024
Available online 5 August 2024

the phenotypical heterogeneity was reproduced considering different scalings, instead of phenotype-specific currents. Since cardiac channelopathies can impact the entire heart or be confined to specific chambers, it is essential to gain a comprehensive understanding of cardiac activity and ion channel functions in both AL and VL hiPSC-CMs. Nevertheless, before investigating cardiac channelopathies using hiPSC-CMs, it is crucial to thoroughly examine their electrophysiological properties, as done in [12], characterizing ionic currents and electrical activity in hiPSC-CMs. Recent findings, [12], highlight significant electrophysiological differences between VL and AL hiPSC-CMs, some of which do not align with those observed in mature human cardiac models.

Nowadays, the employment of maturation techniques highlight the chamber-specific AP phenotype of the cells, [13]. Between developed chamber-specific cultures, atrial ones accurately reflect the electrophysiological characteristics of atrial tissue, which are essential in drug testing scenarios. These atrial-specific cultures enable a more nuanced evaluation of drug responses, especially in the context of AF, atrial-specific arrhythmias or pathologies, providing a valuable platform for assessing the safety and efficacy of pharmaceutical interventions in a chamber-specific manner, [14]. Furthermore, computational models of a diseased tissue could be used to virtually evaluate drugs through a patient-specific model, by paving the way for improving therapeutic targets or ablation techniques. To this end, a phenotype-specific *in-silico* models, for both AL and VL hiPSC-CMs could be useful to realize a virtual platform, which allows to predict the drug effect in a single cell or in cardiac tissue.

In this direction, the latest version of hiPSC-CMs ionic model presented in [15] still provides a developed VL model, while in this work we present the first AL *in-silico* model of hiPSC-CM ionic currents, based on novel experimental data, just published in [1]. First of all, the baseline electrophysiological model is summarized, as well as the mathematical description of atrial-specific additional currents. Moreover, the fine tuning of the model parameters was performed by means of an automatic optimization technique, in order to reproduce realistic AP transient shape and to speed up the parameter tuning phase. Finally, the resulting model was presented and validated against rate dependence and atrial-specific ion current blocking data. By developing this AL hiPSC-CM model, we contribute to bridging the gap in computational models, enabling a more accurate representation and evaluation of drug responses in atrial tissues. This advancement holds promise for enhancing therapeutic strategies and personalized treatment approaches for atrial-specific arrhythmias.

2. Materials and methods

2.1. Experimental data set

In cultures of hiPSC-CMs, the time independent inward-rectifier K^+ current (I_{K1}), that usually maintains negative the membrane diastolic potential (MDP), can be too low or even lacking, leading to unstable MDP, if compared to the mature CMs. These immature electrophysiological conditions correspond to a spontaneous firing activity or a depolarized resting ($\simeq -20$ mV). Dynamic clamp (DC) is a valid and effective approach to overcome immature electrical properties of hiPSC-CM through the injection of a virtual I_{K1} current in a real time mode. DC then leads to a more hyperpolarized MDP allowing the cells to exhibit a more mature AP.

The experimental data set consists of AP recordings from hiPSC-CMs obtained by whole cell patch clamp configuration, in paced condition, with extracellular concentrations $Na^+ = 154.0$, $K^+ = 4.0$, $Ca^{2+} = 2.0$ mM. Experimental data were acquired under controlled temperature and during recordings, the temperature was maintained at 37 °C. iPSCs were obtained by reprogramming adult human dermal fibroblasts of male healthy volunteer. Primary cell lines were derived from a biobank established within previous studies at Cardiocentro Ticino Institute Ente Ospedaliero Cantonale. All studies were approved by the local Ethics Committee (Comitato Etico Cantonale, Bellinzona, Switzerland; Ref. CE 2923) and performed according to the Declaration of Helsinki. The hiPSCs were differentiated into cardiomyocytes and treated with retinoic acid (RA, 1 μM) to induce atrial differentiation, [1,13,16–18]. APs were stimulated at 1 Hz during superfusion of Tyrode's solution: 154 mM NaCl, 4 mM KCl, 2 mM $CaCl_2$, 1 mM $MgCl_2$, 5.5 mM D-glucose, and 5 mM HEPES-NaOH. The pipette solution contained: 23 mM KCl, 110 mM KAsp, 0.4 mM $CaCl_2$, 3 mM $MgCl_2$, 5 mM HEPES-KOH, 1 mM EGTA-KOH, 0.4 mM NaGTP, 5 mM Na_{2ATP}, and 5 mM Na_{2PC}. Analysis of electrical biomarkers have been made on average recording at steady state time point (at least 1 min after). During the experiments, APs, recorded from the hiPSC-CMs, were acquired to drive the numerical formulation of the time independent I_{K1} current (taken from the Koivumäki atrial AP model [19]) in DC. Modelled I_{K1} was calculated in real-time and injected into the myocyte during continued AP recording. All experimental APs data were corrected for the estimated liquid junction potential (a shift of −8 mV was applied), see [20].

Table 1
Experimental data at 1 Hz provided by Altomare et al. in [1]. These biomarkers were also considered for the parameter optimization. Weights used in the automatic optimization process, determined using a heuristic approach and are also summarized in the table.

Biomarkers	Weights in the cost function	Experimental data	
		Mean	Std. Dev.
MDP [mV]	8	−87.11	4.77
APD_{90} [ms]	8	132.47	39.77
APD_{50} [ms]	1	93.61	40.23
APD_{20} [ms]	1	36.06	19.03
$APD_{20/90}$	1	0.26	0.10
V_{max} [mV/ms]	2	101.55	23.8
APA [mV]	1	114.05	8.15

Table 2
Atrial reparametrization of the VL hiPSC-CMs [15]. First set of parameters, scaled according to the specific relation provided in [11]. Setting VL parameters provided in [15] as a starting point, AL values for the presented model can be deduced using the given reparametrization.

	Basic fitting	VL parameter	AL parameter	Units
C_m	$C_{m,v}/1.113$	$C_{m,v} = 98.7109$	$0.887 * C_m = 78.6672$	pF
V_{up}	–	$V_{up,v} = 0.82205$	$0.3924 * V_{up,v} = 0.3226$	mM/s
g_{irel}	–	$g_{irel,v} = 55.808061$	$1.1109 * g_{irel,v} = 75.4190$	mM/s
V_c	–	$V_{c,v} = 8800$	$V_{c,a} = 7012$	μm^3
V_{SR}	–	$V_{SR,v} = 583.728$	$V_{SR,a} = 465.199$	μm^3

The following biomarkers, summarized in Table 1, were considered: diastolic potential MDP, action potential amplitude (APA), AP duration (APD) at 20, 50, and 90% of AP repolarization (APD_{20}, APD_{50}, and APD_{90}), maximum upstroke velocity (V_{max}) and $APD_{20/90}$ (APD_{20} over APD_{90}) ratio selected as the critical biomarker to discriminate AL *versus* VL hiPSC-CM. Notably, the latest parameter, explainable as the APD_{20} normalization, was widely used to characterize the typical triangulation atrial shape and a long plateau ventricular shape and distinguish the two different AP profiles in human working CMs. A cut-off value of this biomarker was defined in [1] using unsupervised learning and it has been pharmacologically validated in a distinct subset of cells.

Each measurement was characterized by its mean value and its standard deviation (Std. Dev.) over a variable number of beats (10–15, at steady-state time point), on a total of 10 cells.

2.2. Atrial parametrization of the VL hiPSC-CMs model

The VL hiPSC-CMs model [15], adapted to the extracellular K^+ concentration of the experimental recordings of Altomare et al. [1],

was used as the baseline to build an atrial specific *in-silico* model for hiPSC-CMs. The matching with the experimental condition $K_o = 4.0\,mM$ affected the reversal potential $E_K = -96.8\,mV$ and ion currents, such as I_{NaK} and I_{Kr}, with effects on the AP duration.

Following the classical Hodgkin–Huxley formalism, the ionic currents through membrane channels were described by the transmembrane potential V_m, the vector of the R gating variables $\boldsymbol{w} = (w^1, \ldots, w^R)$, where R = 18 in [15], and ionic concentrations $\boldsymbol{c} = (Na_i, Ca_i, Ca_{SR})$, where Ca_{SR} means the Ca^{2+} concentration in the Sarcoplasmic Reticulum (SR). This leads to the following system of ODEs.

$$\begin{cases} C_m \dfrac{dV_m}{dt} = I_{ion}\left(V_m, w^1, \ldots, w^R, c^1, c^2, c^3\right) & \text{(a)} \\ \dfrac{d\boldsymbol{w}^r(t)}{dt} = m_w^r\left(V_m, w^1, \ldots, w^R\right) \qquad r = 1, \ldots, R & \text{(b)} \\ \dfrac{dc^s(t)}{dt} = m_c^s\left(V_m, w^1, \ldots, w^R, c^1, c^2, c^3\right) \quad s = 1, 2, 3 & \text{(c)} \end{cases} \tag{1}$$

where C_m is the membrane capacitance and I_{ion} is the sum of 13 membrane currents and the stimulus current.

As a first step towards the atrialization we rescaled 11 parameters of the VL hiPSC-CMs model [15] by factors provided by the literature and summarized in Table 1 of [11]. Among them, two different sets can be identified. The first one corresponds to parameters for which a specific relation between VL and AL phenotype is provided in the literature, since they do not derive from data fitting. The corresponding values of this first set in [15] are now the ventricular parameters, used to evaluate the atrial one through the proposed scaling in [11]. In the second set, parameters were derived by fitting a mixed pool of voltage clamp data, affected by phenotypical heterogeneity. There, the resulting basic fitting parameters were scaled through functions f_a, f_v to the AL or VL versions. In our case, basic fitting parameters needed for the rescaling, are computed through the inverse function f_v^{-1} from the VL value provided in [15]. Some of these changes are summarized in Table 2, while parameters not appearing in the table will feed the optimization process, detailed in Section 2.4.

2.3. Additional atrial-specific currents

The parental AL model proposed in [11] was based on mixed recordings, thus any atrial-specific current could be considered into the model. Several membrane currents are only expressed in the atria and we considered the integration in the new AL model of the ultrarapid delayed rectifier current (I_{Kur}) and the small conductance Ca^{2+} activated K^+ (SK) channel (I_{KCa}).

2.3.1. Ultrarapid delayed rectifier current formulation

The outward I_{Kur} is the first atrial-specific additional current we integrated into the model, since it plays a significant role in human atrial repolarization and is generally characterized by rapidly activation, and slow and partial inactivation. Due to atrial-specific expression, the pharmacological inhibition of I_{Kur} takes into account the selective atrial APD prolongation with minimal adverse effects in the ventricles.

We considered the Courtemanche's formulation described in [21] written as follows:

$$\begin{aligned} I_{Kur} &= g_{Kur} \cdot u_a^3 \cdot u_i \cdot \left(V_m - E_K \cdot 10^3\right) \\ g_{Kur} &= \text{coeff}_{\text{Kur}} \cdot \left[0.005 + \frac{0.05}{1.0 + \exp\left(-\frac{V_m - 15.0}{13.0}\right)}\right], \end{aligned} \tag{2}$$

where g_{Kur} is the maximum conductance and $\text{coeff}_{\text{Kur}}$ is an additional rescaling factor assumed to be equal to 1. The current dynamic is defined by two specific gating variables, u_a, u_i, with an Hodgkin–Huxley first order dynamic described by the following equations, where $K_{Q,10} = 3$:

$$\alpha_{u(a)} = 0.65\left[e^{-\frac{V_m+10.0}{8.5}} + e^{-\frac{V_m-30.0}{59.0}}\right]^{-1}$$

$$\beta_{u(a)} = 0.65 \cdot \left[2.5 + e^{-\frac{V_m+82.0}{17.0}}\right]^{-1}$$

$$\tau_{u(a)} = \frac{K_{Q,10}}{\alpha_{u(a)} + \beta_{u(a)}}$$

$$u_{a(\infty)} = \left[1.0 + e^{-\frac{V_m+30.0}{9.6}}\right]^{-1}$$

$$\frac{du_a}{dt} = \frac{u_{a(\infty)} - u_a}{\tau_{u(a)}}$$

$$\alpha_{u(i)} = \left[21.0 + e^{-\frac{V_m-185.0}{28.0}}\right]^{-1}$$

$$\beta_{u(i)} = e^{-\frac{V_m+158.0.0}{16.0}}$$

$$\tau_{iur} = \frac{K_{Q,10}}{\alpha_{u(i)} + \beta_{u(i)}}$$

$$u_{i(\infty)} = \left[1.0 + e^{-\frac{V_m-99.45}{27.48}}\right]^{-1}$$

$$\frac{du_i}{dt} = \frac{u_{i(\infty)} - u_i}{\tau_{u(i)}}$$

Finally, initial conditions for the new gating variables are given in Appendix B.

2.3.2. Small conductance Ca^{2+} activated K^+ channel

The second additional current we take into account is I_{KCa}, presented by Skibsbye in 2016, [22]. SK channel opening is described as a two-state Markov model. The opening of the channel simply depends on the sub-sarcolemmal Ca^{2+} concentration, Ca_i. The equations proposed for the opening of the channel are:

$$KCa_{on} = 47.0 \cdot 10^6$$

$$KCa_{off} = 13.0$$

$$\frac{dO}{dt} = (1 - O) \cdot KCa_{on} \cdot Ca_i^2 - O \cdot KCa_{off}$$

where O is the opening gating variable. The resulting current equation is

$$I_{KCa} = g_{KCa} \cdot O \cdot \frac{V_m - E_K \cdot 10^3}{1 + \exp\left(\frac{V_m - E_K \cdot 10^3 + 120.0}{45.0}\right)}, \tag{3}$$

where the maximum conductance is $g_{KCa} = 0.072\ \left[\text{nS/pF}\right]$.

2.3.3. Time independent inward-rectifier K^+ current formulation

As described in the first section, RA-treated CMs were simulates using the DC protocol to overcome the limitation of the low I_{K1} expression in immature hiPSC-CM, as described in [1,23]. Since the model has to be consistent with experimental data we are trying to replicate *in-silico* the injection of I_{K1} current, changing the arbitrarily proposed formulation. Among the two state-of-the-art I_{K1} *in-silico* currents injected in DC mode [1], we integrated in the model the human atrial specific I_{K1} formulation published in 2011 by Koivumäki et al. [19], and in 1998 by Nygren et al. [24]. I_{K1} current, responsible for the late repolarization phase, is thus described by the following equation:

$$I_{K1} = g_{K1} \cdot K_i^{0.4457} \cdot \frac{V_m - E_K}{1 + e^{1.5(V_m - E_K + 3.6)F/RT}} \tag{4}$$

where $g_{K1} = 0.0765\ \left[\text{nS/pF}\right]$, F is the Faraday's constant, R is the gas constant and T is the absolute temperature.

2.4. Parameter optimization

The resulting model, extended with additional atrial-specific currents was used as a baseline model. Firstly, we manually increased

Table 3
Optimized parameters. We provide the complete set of parameters chosen for manual or automatic optimization. Lower and upper boundaries are provided for the automatic tuning only.

	Parameter	Starting value	LB	UB	Optimized value	Units
Manual tuning	g_{Kr}	29.86	–	–	16.8723	S/F
	g_{K1}	0.15	–	–	0.169	nS/pF
	g_{bNa}	1.14	–	–	0.114	S/F
	RyR_{a1}	0.05169	–	–	0.1034	μM
	$\text{coeff}_{\text{Kur}}$	1	–	–	3.5	–
Automatic tuning	g_{Na}	$1.1116 \cdot 10^4$	$8.1701 \cdot 10^3$	$1.5173 \cdot 10^4$	$9.8001 \cdot 10^3$	S/F
	g_f	22.276	15.5934	28.9592	25.9	S/F
	g_{CaL}	$8.6 \cdot 10^{-5}$	$6.045 \cdot 10^{-4}$	$1.1226 \cdot 10^{-4}$	$7.45 \cdot 10^{-5}$	S/F
	g_{to}	59.8	41.8653	77.7499	59.45	S/F
	g_{Ks}	2.041	1.4287	2.6533	2.0856	S/F
	g_{PCa}	0.412	0.2887	0.5363	0.4570	S/F
	g_{NaL}	$2.3 \cdot 7.5$	12.0750	22.425	13.3509	S/F
	g_{KCa}	0.072	0.0504	0.0936	0.0754	S/F
	k_{NaCa}	$3.26 \cdot 10^3$	$2.2801 \cdot 10^3$	$4.2344 \cdot 10^3$	$3.4507 \cdot 10^3$	A/F
	P_{NaK}	2.192	1.5357	2.8521	2.2718	A/F

and calibrated: *(i)* the maximal conductance g_{K1} in the novel I_{K1} formulation, mostly responsible of the shortening of the APD_{90} and the hyperpolarization of the MDP, *(ii)* K^+ driven currents I_{Kr} and I_{Kur} affecting the fast repolarization phase, through the maximal conductance g_{Kr}, and the additional scaling factor $\text{coeff}_{\text{Kur}}$ in Eq. (2), *(iii)* the maximal conductance g_{bNa} and the adaptation gate constants of the release RyR_{a1} in order to restore intracellular Ca^{2+} and Na^+ concentrations to physiological ranges and prevent the cell from accumulating Ca^{2+} in the SR. Secondly, voltage-dependent inactivation time constants τ_{f1}, τ_{f2} in I_{CaL} inactivation gating variable f_1, f_2 where updated in order to shift the recovery from inactivation towards more negative values of V_m.

$$\tau_{f2} = 600e^{-\frac{(V_m+\mathbf{50})^2}{\mathbf{400}}} + \frac{31}{1+e^{\frac{25-V_m}{10}}} + \frac{\mathbf{1}}{1+e^{\frac{30+V_m}{10}}}$$

$$\tau_{f1,s} = 20 + 1102.5e^{-\frac{(V_m+\mathbf{50})^2}{15}} + \frac{200}{1+e^{\frac{13-V_m}{10}}} + \frac{\mathbf{280}}{1+e^{\frac{30+V_m}{10}}}$$

$$\tau_{f1} = \tau_{f1,s} \cdot \mathbf{C_{f1}}$$

$$\mathbf{C_{f1}} = \begin{cases} \mathbf{1.35}\cdot\left[1 + 1433 \cdot \left(Ca_i - 50 \cdot 10^{-6}\right)\right], \text{if } \frac{df1}{dt} > 0 \\ 1, \text{ otherwise} \end{cases}$$

Bold values are resulting optimized parameters.

Finally, we performed the parameter optimization using a hybrid approach, combining a genetic optimization and a simplex optimization, as described in [25]. The first step solves the unconstrained optimization problem using the Matlab function *gamultiobj*, which finds the minimum on the Pareto Front of the cost function. It is based on a genetic algorithm which mimics the natural selection process in biological evolution, iteratively modifying a population of individual solutions. The second step is based on the Matlab *fminsearchbnd* function, which effectively implements the Nelder–Mead Simplex Method and finds the minimum of a unconstrained multivariable cost function using a derivative-free method. The resulting hybrid method minimized the cost function, built on the experimental biomarkers we want to simulate. The chosen *in-vitro* biomarkers are the same provided in [1] and they are reported also in Table 1. The cost function structure is defined by the following equations:

$$\begin{aligned} Cost &= \sum_1^N w_i \cdot Cost_i \\ Cost_i &= \frac{\left(b_i - LB_i\right)^2 \mathbb{1}_{\{b_i<LB_i\}} + \left(b_i - UB_i\right)^2 \mathbb{1}_{\{b_i>UB_i\}}}{0.5 \cdot |LB_i + UB_i|} \end{aligned} \quad (5)$$

where b_i is the ith biomarker, N the number of biomarkers used, w_i the weight for each biomarker's cost and LB_i, UB_i the lower and the upper bound respectively for the considered biomarker i. Each bound depends on the experimental standard deviation of the single biomarker. Parameters were chosen to include all the main ionic conductances and can be listed as follows: *(i)* the maximum conductances of I_{Na}, I_f, I_{CaL}, I_{to}, I_{Ks}, I_{pCa}, I_{NaL}, I_{KCa}, *(ii)* k_{NaCa}, P_{NaK}. The parameter values were constrained in a range $[-30\%, +30\%]$ with respect to their starting value, given in the VL hiPSC-CMs model [15] or as a result of its atrial parametrization described in the previous section, in order to avoid non-physiological values, such as negative conductances.

Biomarkers were computed at the steady state (after 800 s) as the average of the last 2 beats. Results are summarized, both for the manual tuning and the automatic optimization, in Table 3.

2.5. Numerical simulation setting

Our model was implemented in MATLAB (The MathWorks, Natick, MA). Numerical integration was performed using a solver for stiff systems (ode15s), with an initial step size of $2 \cdot 10^{-5}$ s and a maximum step size of 1 ms. To accurately reproduce experimental condition and the external stimulus applied to the cell, an additional current I_{stim} (amplitude 1.41 nA, duration 2 ms) was applied in the model with the frequency of 1 Hz. Simulations were always conducted at steady state, reached after 800 s of simulations. The resulting initial conditions at steady state are summarized in Appendix A. Conversely, to test the APD dependence on the applied pacing rate, we paced the AL model at 1, 1.5, 2 and 4 Hertz, cycle length (CL) 1000, 750, 500 and 250 ms respectively, for 800 beats to reach the steady state. To test the current block effect the model was paced setting the frequency equal to 1 Hz.

3. Results

3.1. The new AL hiPSC-CMs model

The introduction of atrial-specific ionic currents and the subsequent automated optimization process successfully identified a new phenotype-specific AL ionic model. A schematic diagram of our AL hiPSC-CM model is reported in Fig. 1, showing the cell structure: the model includes two compartments, namely cytosol and Sarcoplasmic Reticulum SR, as well as the main ion channels, exchangers and pumps. The model follows the classical Hodgkin–Huxley formulation, which describes the transmembrane potential through the ODEs system Eq. (1), where R = 21. There, I_{ion} is the sum of 15 ion currents, exchangers and pumps (see Fig. 1), accurately reported in Appendix A. All model equations and parameter values are provided in Appendix B. In Fig. 2 simulated paced AP trace and Ca^{2+} transients at steady state in paced conditions are reported, together with the 15 ionic membrane currents, and the fluxes from the SR.

In the upper panels, below the AP traces, the additional currents and the innovative formulation are depicted: I_{Kur} is responsible for the more prominent initial repolarization; I_{KCa}, which takes part in setting the cardiac diastolic potential phase 4 of the AP; I_{K1} belongs to the family of classical inward rectifiers, meaning that it presents a peak

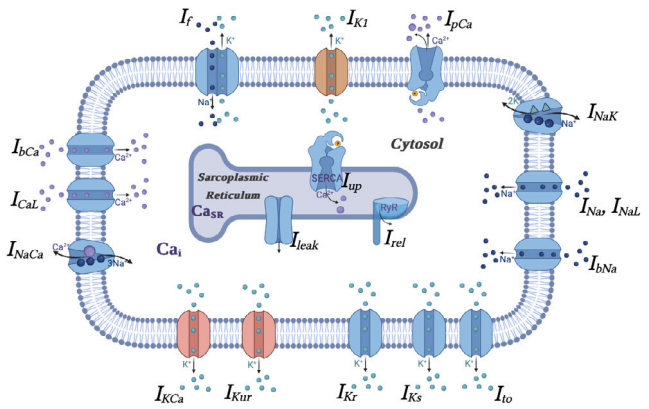

Fig. 1. Schematic diagram of the AL hiPSC-CM model depicting cell compartments and the major functional components and the 15 membrane currents. Fluid compartments include cytosol and SR. Ca^{2+}-handling is described by: I_{up} uptaking Ca^{2+} by SR, I_{rel} releasing Ca^{2+} by ryanodine receptors (RyR) and I_{leak}. Pink and brown channels stand for additional atrial-specific currents or with a different formulation, respectively.

Table 4
Biomarkers matching. Experimental and simulated values of the biomarkers considered for the parameter optimization. Experimental data are provided as Mean ± Std. Dev., from [1]. AP biomarkers resulting from the *in-silico* model, are in agreement with the *in-vitro* variability range.

Biomarkers	Experimental data	Simulated values
MDP [mV]	−87.11 ± 4.77	−92.70
APD_{90} [ms]	132.47 ± 39.77	148.94
APD_{50} [ms]	93.61 ± 40.23	96.94
APD_{20} [ms]	36.06 ± 19.03	26.6012
$APD_{20/90}$	0.26 ± 0.10	0.1786
V_{max} [mV/ms]	101.55 ± 23.8	122.503
APA [mV]	114.05 ± 8.15	136.53
Int90 [mV s]	10.099 ± 4.012	11.621

at the beginning of the resting phase 4, to conduct inward K^+, while outward conductance is voltage-dependently blocked by intracellular polyvalent ions of the cytoplasm.

The automated optimization process described in Section 2.4 successfully provides a new set of parameters for our new AL model. Fig. 3 illustrates the simulated AP and traces from 18 illustrative cells: the comparison highlights that the simulated AP contour overlap on average experimental traces. The simulated AP biomarkers at steady state in paced conditions fall within the confidence interval of the experimental data (except for the APA, highly dependent on the stimulus current), confirming the reliability and accuracy of our model predictions. *In-vitro* AP biomarker variability ranges, provided as Mean±Std. Dev. in [1], are reported in the last column of Table 4. An additional integral biomarker is considered in order to avoid the intrinsic variability. The membrane potential integral is defined as in [26]:

$$\text{Int90} = \int_{t_1}^{t_2} [V_m - V_m(t_1)]\, dt \tag{6}$$

where t_1 and t_2 are here time points corresponding to when V_m is 90% below the maximum value during the depolarization and repolarization phases of the AP. Experimental data is derived from each trace and the simulated values fall within the confidence interval.

3.2. Non-mature AL hiPSC-CMs conditions

As discussed in the experimental setup, Section 2.1, DC technique allows the cells to reach a stable hyperpolarized MDP in resting conditions and then a physiological AP waveform. During this electronic maturation process, the cell progresses through multiple stages, since the initial unstable depolarized MDP is driven through spontaneous activity and finally reaches its resting value.

As a first result, we require our ionic model in unpaced conditions to mimic the maturation process, reaching a stable hyperpolarized MDP. Once a stable resting value is achieved, then it is possible to apply the stimulation protocol and derive the novel AL hiPSC-CMs model. As depicted in Fig. 4, the progression of different maturation stages is replicated by the unpaced *in-silico* model at different I_{K1} densities. Indeed, the immature condition with spontaneous oscillations between depolarized values, corresponds to small percentages of the injected current ($g_{K1} \leq 0.02$ [nS/pF]), while the spontaneous firing activity arises for $g_{K1} \in [0.03, 0.06]$ [nS/pF]. We also note that increasing g_{K1} values also leads to the increase of the spontaneous firing cycle length. Finally, for values greater or equal than 0.07 [nS/pF], the current injection leads to an hyperpolarized MDP.

3.3. Rate dependence

The dependence of APD on pacing rate is a fundamental property of CMs that, when altered, may promote life-threatening cardiac arrhythmias. In order to validate the new hiPSC-CM model after the introduction of the new atrial-specific currents formulation and the parameters optimization by means of our AP data, we tested the model capability to simulate the APD rate dependence.

To test the APD dependence on the applied pacing rate, the model has been run following the protocol depicted in the previous section, considering different frequencies of stimulation, i.e. CL = 1000, 750, 500, 250 ms. We then compare simulated APD at 90, 50 and 20% of repolarization with the available *in-vitro* data in [1]. The novel AL model simulations show a qualitative agreement with the experiments and traces of Altomare et al. [1], as shown in Fig. 6. The simulated rate dependency values (diamonds in Fig. 5) are close to the experimental average values (circles), falling within the experimental error bars depicted in Fig. 5. A quantitative comparison summarized in Table 5 highlights that APD_{90} and APD_{50} simulated values as well as the integral index Int90 fall within the confidence interval of the experimental data. Nevertheless APD_{20} is lower at the highest pacing rates, and this minimal discrepancy is probably due to the APD_{20} dependency on the applied I_{stim} amplitude.

3.4. 4–AP drug test

I_{Kur} current is one of the atrial-specific currents added to our model. It plays a significant role in human atrial repolarization and is generally characterized by rapidly activation, and slow and partial inactivation. Due to atrial-specific expression, the pharmacological inhibition of I_{Kur} takes into account the selective atrial APD prolongation with minimal adverse effects in the ventricles.

In order to compare the novel AL model with the experimental data, we challenged our model by exploiting the sensitivity of atrial I_{Kur} current to a selective blocker 4–aminopyridine (4–AP, 50 μM). In both isolated human adult atrial CMs and single atrial hiPSC-CM the blocking of the I_{Kur} resulted in APD_{90} prolongation [17,18]. As expected, in *in-vitro* experiments 4–AP superfusion causes the prolongation of AP in AL hiPSC-CMs. Analysis of 4–AP effects in APD changes (summarized in Table 6) showed that the highest prolongation was detected in the APD_{20} phase, where the I_{Kur} mostly contributed during the electrical activity of AL CMs.

We simulated I_{Kur} block by 50 μM of 4–AP as a 80% block of I_{Kur} maximum conductance, as suggested for human adult CMs in [27]. Similar values were published in [28] for human CMs, where dose–response curves show a 80% current block with 4–AP concentration of 50 μM. Human adult CMs are used as a reference since any information is provided about the I_{Kur} density in isolated hiPSC-CMs. Indeed, genes encoding for the I_{Kur} channel subunits are absent in the early phase of heart embryogenesis and are finely tuned in the developing heart, see [1]. Similarly, we expect that differentiating hiPSC-CM express

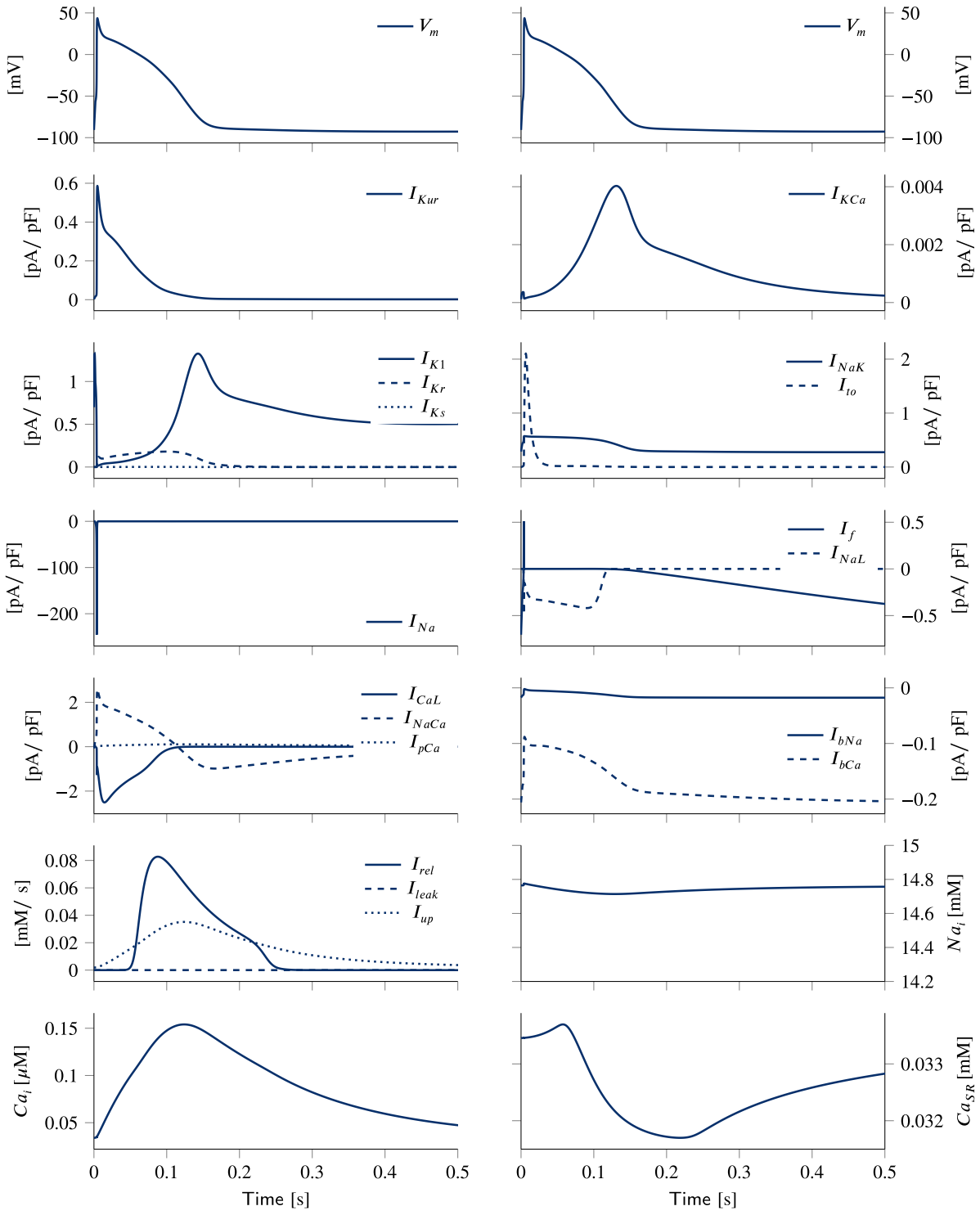

Fig. 2. Steady state ionic currents and ionic concentrations dynamic. Ionic currents dynamic, fluxes from the SR, and evolution over time at steady state of the intracellular Na^+ and Ca^{2+} concentrations and Ca^{2+} concentration in the SR in paced conditions. In the upper panels the transmembrane potential is reported as a reference.

mixed set of ion channels that affect the repolarization phase of AP in response to specific drug.

Our simulations suggest that I_{Kur} block induces an APD prolongation, in agreement with experimental results, as shown in Fig. 7. Furthermore, the quantitative comparison of APD on different AP phases in Table 6 validates the accuracy of the *in-silico* model, since every value APD change (delta %) is in the experimental variability range. Finally, also the higher contribution in the APD_{20} phase is preserved (36%).

4. Discussion

Research on hiPSC-CMs is rapidly developing, with new experimental data becoming available, which in turn drives the evolution of computational models and more accurate *in-silico* tools. As for adult cardiac cells, which show different AP shapes according to their location and specialization in the heart, hiPSC-CMs show different AP morphologies, that are usually categorized as VL, AL, or nodal-like. The focus on electrophysiological characteristics exhibited by AL cells allows a

Table 5
Rate dependence. Simulated (Sim.) values with different pacing rates, and experimental (Exp.) data provided as Mean ± Std. Dev., from [1]. A quantitative comparison highlights that APD_{90} and APD_{50} simulated values fall within the experimental confidence intervals.

Biomarkers	CL = 1000 ms		CL = 500 ms		CL = 250 ms	
	Exp. data	Sim.	Exp. data	Sim.	Exp. data	Sim.
APD_{90} [ms]	138.65 ± 38.89	148.94	115.79 ± 28.24	129.8	89.55 ± 19.17	100.1
APD_{50} [ms]	99.80 ± 38.93	96.94	81.33 ± 27.75	80.85	58.30 ± 16.22	52.68
APD_{20} [ms]	41.27 ± 21.10	26.60	33.82 ± 16.94	14.85	21.45 ± 8.69	9.71
$APD_{20/90}$	0.28 ± 0.10	0.18	0.31 ± 0.13	0.114	0.24 ± 0.07	0.09
APA [mV]	115.98 ± 7.99	136.5	115.02 ± 9.91	129.85	109.95 ± 8.67	132.1
Int90 [mV s]	10.099 ± 4.012	11.621	8.251 ± 2.922	9.74	5.908 ± 1.753	6.713

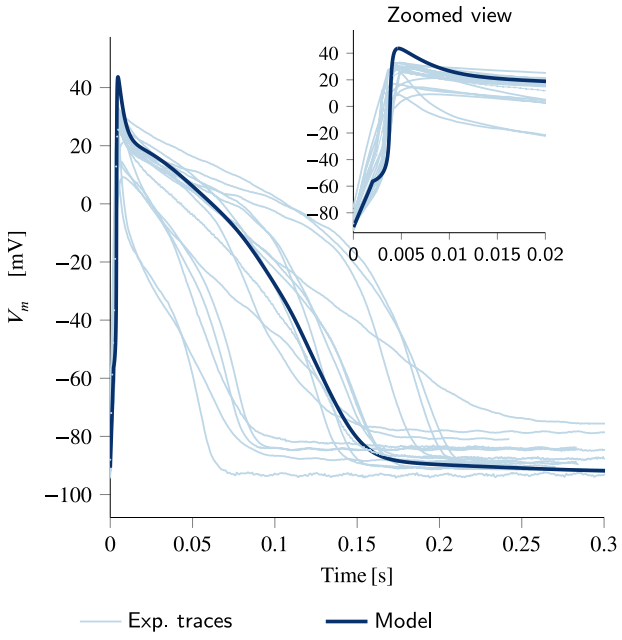

Fig. 3. Simulated AP overlapped with experimental traces. Illustrative experimental AP from 18 cells (light blue) and the AP simulated by the AL hiPSC model (dark blue). The comparison highlights that the simulated AP contour overlap on average experimental traces.

Table 6
4–AP effect on different AP phase. Experimental and simulated values of the biomarkers when considering 4–AP treatment. Experimental data provided as Mean ± Std. Dev. in the form of Delta %, from [1].

Biomarkers	Experimental	Simulated	Simulated absolute values	
	delta %	delta %	Without 4AP	With 4AP
APD_{90} [ms]	19 ± 21.187	17.19	148.94	174.5
APD_{50} [ms]	36.4 ± 37.63	20.09	96.94	116.41
APD_{20} [ms]	56.8 ± 63.87	36.2	26.60	36.2
$APD_{20/90}$	0.3 ± 0.31	15.9	0.179	0.207

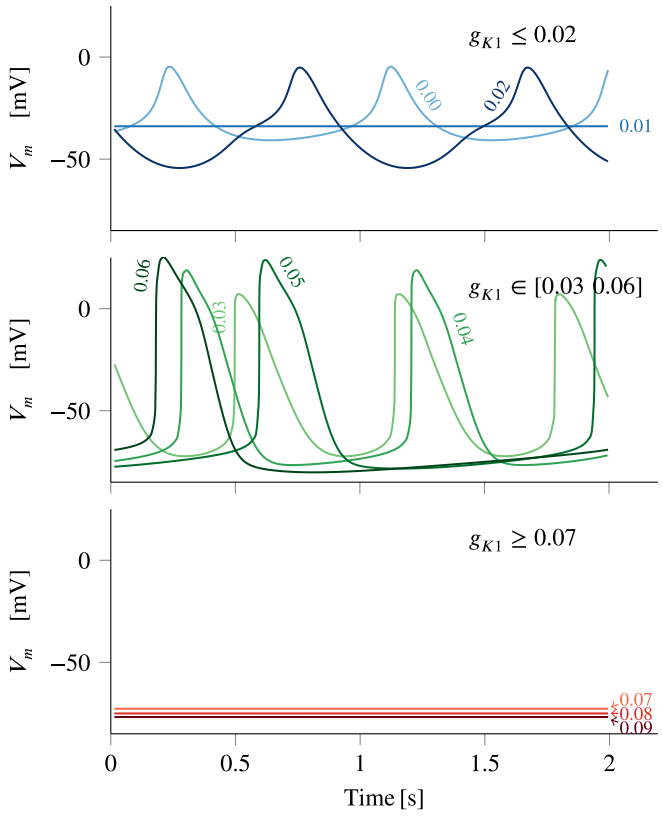

Fig. 4. AP morphology with respect to the g_{K1} variability. The gradual increase of I_{K1} current injection drives the cell from the initial unstable depolarized MDP (blue dashed lines) to the mature hyperpolarized resting values (red dotted lines), passing through non-mature spontaneous beating (green solid lines). Absolute values of g_{K1} ([nS/pF]) are displayed near the associated simulated curve.

deeper understanding of the mechanisms underlying chamber-specific cardiomyopathies.

The present work aimed at developing a highly specific AL hiPSC-CM model tailored to the distinct phenotype observed in atrial cells, thus contributing to elucidate the intricacies of atrial AP electrical abnormalities and to acknowledge the broader implications for personalized medicine. In particular, modelling studies can play an important role in advancing personalized drug testing methodologies, see e.g. [26,29,30].

Starting from the original hiPSC-CMs model [11], the works Koivumäki et al. [31] and Kernik et al. [32] provided novel insight and material for the subsequent VL hiPSC-CM model [15]. As suggested in [33], Koivumäki formulation employs a complex layered compartmental structure, which increases the computational cost of model simulations. Conversely, Kernik automaticity is sustained by a different I_{CaL} formulation, rather than being directly sustained by the Ca^{2+} handling dynamic. For these reasons, we started developing our new AL hiPSC-CMs model using the ventricular hiPSC-CM model [15] as a parent model. We remark that [15] also shows the predictive power of these models through an *in-silico* trial on different drugs, in agreement with *in-vitro* data sets.

Our new AL hiPSC-CMs model better recapitulates the phenotypical atrial specificity of cardiomyocytes. As shown in Fig. 8, the presented model can fit experimental APs, while the parent hiPSC-CMs models (the VL version [15] in red and the AL version [11] in green) are far away from the experimental traces.

We have developed our AL hiPSC-CM model using literature data in order to identify the ionic currents most likely contributing to VL and AL AP differentiation in adult CMs. Because of the clinical interest in AF, we considered various K^+ channels usually remodelled during AF simulations. Several of them are almost only expressed in the atria and

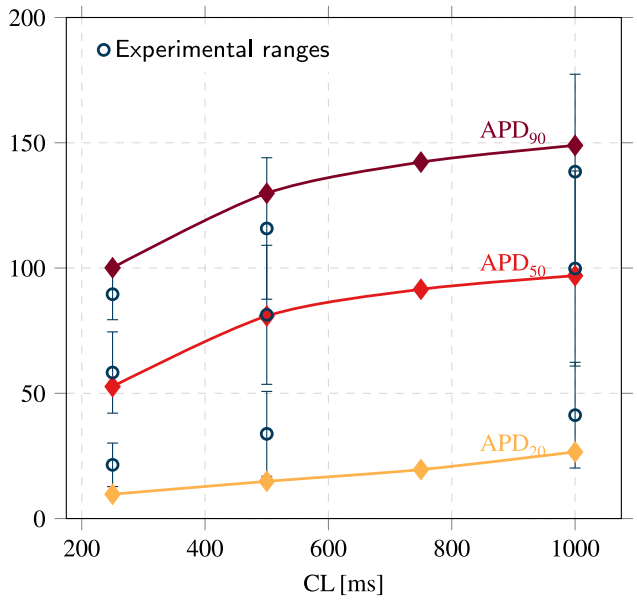

Fig. 5. Rate dependence curves. Simulated APD_{90}, APD_{50}, and APD_{20} rate dependence curves (diamonds) produced by the novel AL model compared with *in-vitro* experimental data: average value (circles) and variance (vertical error bars). Values are in milliseconds.

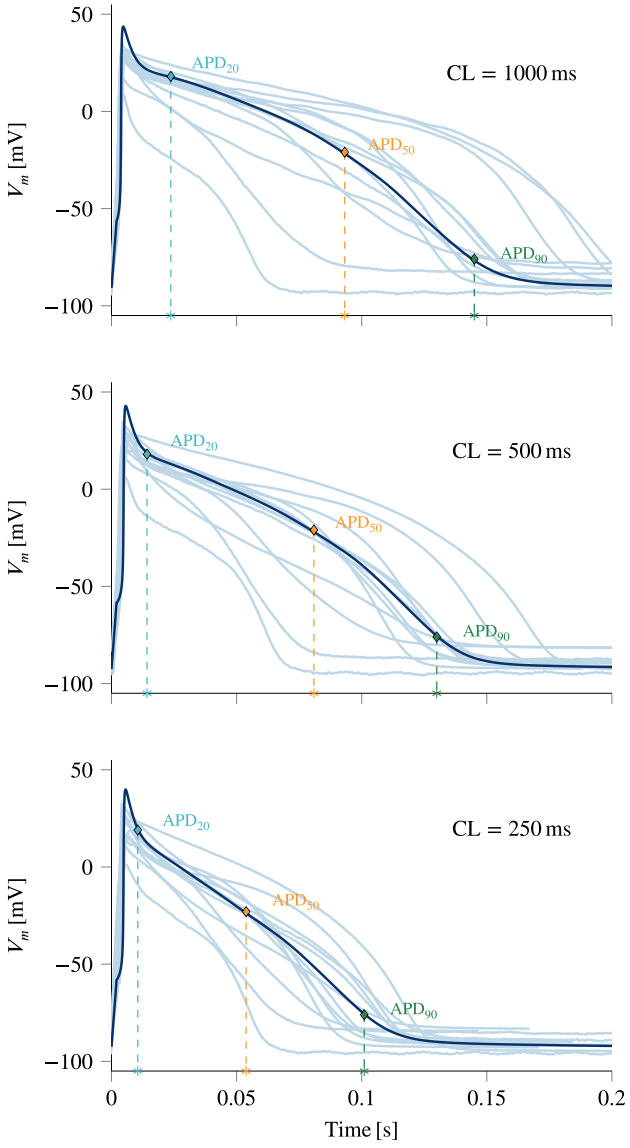

Fig. 6. Experimental rate dependence traces. Illustrative experimental AP from 13 cells (light blue) and the AP simulated by the AL hiPSC model (dark blue) when considering three different frequencies (CL = 1000, 500, 250 ms). Increasing frequencies reduces both experimental and simulated APDs.

they are summarized in [34]. Among them, we incorporated the atrial-specific I_{Kur} and I_{KCa} currents. Recent studies, such as [35,36], suggest that native I_{Kur} density in AL hiPSC-CMs is substantially smaller than the I_{Kur} density of freshly isolated human atrial myocytes and a DC approach for the injection of virtual I_{Kur} current could lead the cell to a more adult phenotype. Further studies are required to investigate *in-silico* the impact of an additional I_{Kur} current, also taking into account different formulations, such as Maleckar et al. [37].

Conversely, we did not take into account two other currents: *(i)* the Acetylcholine-sensitive K^+ current ($I_{K,ACh}$) and *(ii)* the Two-pore-domain K^+ (I_{K2P}) current. *(i)* $I_{K,ACh}$ is an atrial specific current activated by the neurotransmitter acetylcholine (ACh) after binding to the specific muscarinic receptor. Mathematical formulations for this current have been provided for rabbit sino-atrial node cells, [38], and for human atrial cells, [39]. In both these current formulations, $I_{K,ACh}$ depends on the ACh concentration, being null if [ACh] is zero. Since the ACh concentration in control conditions is unknown, the $I_{K,ACh}$ contribution to the AP in *in-vitro* isolated hiPSC-CMs can be neglected. Nevertheless, this current could be investigated experimentally in hiPSC-CMs and incorporated into future modelling studies. *(ii)* The I_{K2P} current described in Schmidt's model [40] is positively modulated in the paroxysmal AF and is overexpressed in the chronic AF. However, in basal conditions the current does not concur to the electrical activity of a healthy patient with sinus rhythm and, therefore, we did not include it in the present study.

Furthermore, we choose to change the I_{K1} formulation, inspired by the Koivumäki 2014 [19] model of human adult atrial CM. This latter change was implemented mainly to correctly take into account the use of DC technique in the experimental setup based on the injection of the Koivumäki I_{K1} current to help the electronic maturation of *in-vitro* hiPSC-CMs, [1].

In order to keep the new model consistent with experimental data and fit different parameters, we have performed an optimization procedure minimizing a cost function built with the same biomarkers and experimental ranges provided by Altomare et al. [1]. The tuned parameters are listed in Table 3. The result is a new AL hiPSC model where APs' features in paced conditions match the Altomare et al. experimental dataset, as depicted in Fig. 3. The comparison between the experimental and simulated AP features reported in Table 4 shows how the model is matching well the real APs. In particular, the AL model satisfies the discriminating rule defined in [1], based on defined cut-off value for the for $APD_{20/90}$ ratio. According to this rule, an AL phenotype is detected when $APD_{20/90} \leq 0.44$. The only relevant discrepancy in Table 4 can be found in the APA biomarker, with percentages of discrepancy equal to 10%. The mismatching in APA can be attributable to the high sensitivity of this biomarker to the external applied stimulus.

Our model was validated against the available experimental data ranging over three different pacing frequencies. The *in-vitro* experimental data set was not used in the optimization process, but the novel AL hiPSC model well replicates the rate dependence curve, if considering the APD_{50} and APD_{90}, as depicted in Fig. 5. The comparison between the provided and resulting AP features reported in Table 5, and qualitatively shown in Fig. 6, confirming that our model is matching well the experimental range of values. Also, the APD_{20} rate dependence curve qualitatively overlap with the experimental data, even if an accurate

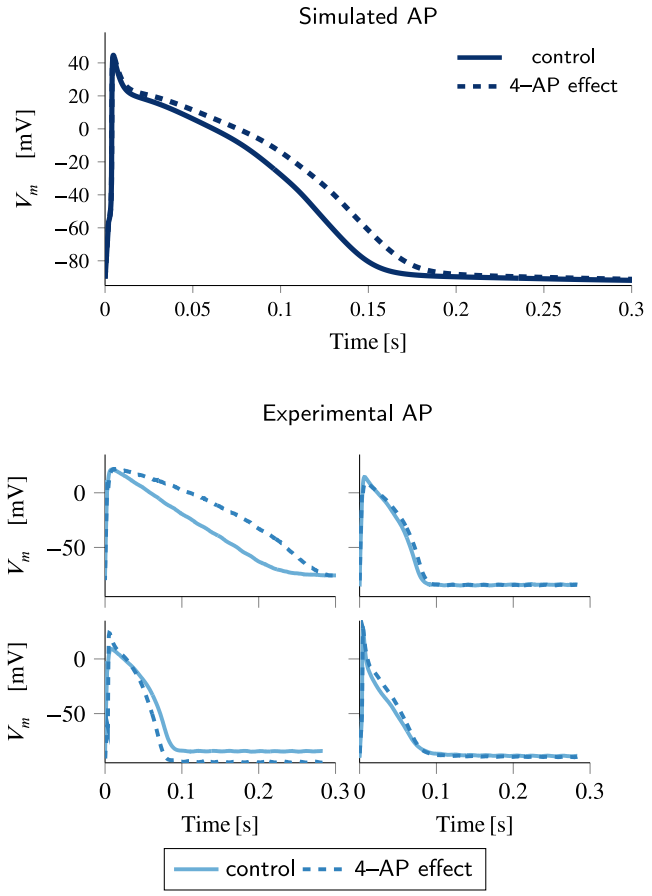

Fig. 7. 4–AP effect. Illustrative experimental AP from four cells (bottom panels, with light blue traces) and the AP simulated by the AL model (upper panel, with dark blue traces), when considering the control (solid line) or the 4–AP effect (dashed line).

quantitative comparison (Table 5) shows some minimal discrepancies for CL = 500 ms and CL = 250 ms.

We also validated our model when considering the response to the I_{Kur} atrial-specific current blocker 4–AP under an external stimulus; thus the simulation results were validated against the corresponding *in-vitro* experiments, which were not used during the optimization process (see Table 6). The rational for this choice is to show the key role of the I_{Kur} current in AL hiPSC-CM cells (and AL hiPSC models as well). Our novel AL hiPSC *in-silico* model accurately replicates the effect of current blocker on the AP shape and the resulting APD prolongation, confirming the phenotype specificity of *in-vitro* cells. In future works, we aim to test the rate dependence of the effects of I_{Kur} on AP repolarization in hiPSC-CMs.

To sum up, in this work we present an updated and more specific version of an AL hiPSC-CM *in-silico* model, based on a new dataset of electrophysiological data and novel technologies to improve the cell maturation. Due to its relatively light formulation (25 ODEs), our model is suitable also for very large studies on *in-silico* populations, and future works will explore the possibility to support screening of different phenotype specific drugs at various concentrations. Indeed, our model is also suitable to be the baseline for population-based studies (see [41,42]), where an initial large population will be created with randomly varied parameter sets, and will be calibrated to retain only those models that are fully consistent with the experimentally observed ranges. The calibration process will reduce the population to a lower number of accepted models, representing control and mutant populations for different cardiac diseases, targeting the assessment of

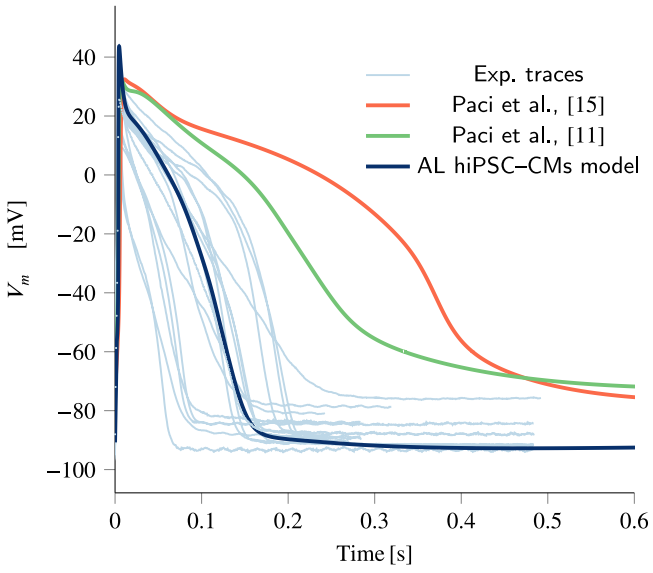

Fig. 8. Illustrative experimental AP from 18 cells (light blue) overlapped with simulated APs from three different models. The plot shows that the presented AL hiPSC-CMs model falls within the range of experimental traces.

the electrophysiological effects of a drug cardiotoxicity (for further details see [43]).

Among the different scenarios, different phenotypes, including sinoatrial nodes cells, can be explored since intrinsic pacemaker properties can be simulated when considering $g_{K1} \in [0.03, 0.06]$, as shown in Fig. 3. Indeed, both the funny current (I_f) and the Na^+/ Ca^{2+} exchanger current (I_{NaCa}) are included into the model (see Fig. 2 and Appendix B), playing a pivotal role in sustaining the automaticity of AP.

In the direction towards pathological conditions and arrhythmias, we observe that CM in pulmonary vein (PV) sleeves are important in AF, and share with AL hiPSC-CMs some AP features, such as the downregulation of some currents with respect to the rest of the atrial body and the shorter AP. PVs have different ionic current properties compared to left atrium and distinct electrophysiological properties related to different densities of several ionic currents with pulmonary vein inward-rectifier currents being smaller and delayed-rectifier currents larger than in left atrium. To mimic PVs behaviour, we followed the suggestions in [44] and we considered an increase of 50% of the inward rectifier I_{Ks}, and a reduction of 50% of both the transient outward K^+ current I_{to} and the L-type Ca^{2+} current I_{CaL}. Differences, such as the shorter APD in PVs, are highlighted in Fig. 9.

Furthermore, measurements of extracellular field potentials through multi-electrode arrays system from a network of hiPSC-CMs have recently garnered significant attention for their applications in disease modelling, [45]. This innovative technique offers a powerful means to bridge the gap between single-cell electrical properties and multicellular tissue-like models.

4.1. Limitations

Our work was based on a unique source of experimental data by Altomare et al. [1], since this work was the most comprehensive report about AL hiPSC-CMs maturation, classification and AP response to drugs. It must be noted that extensive experimental data sets from healthy mature hiPSC-CMs are nonexistent because different technologies for generating mature AP waveform are still under evaluation. We considered DC as a consolidated technique (see [36,46,47]), but new experimental data should be provided to improve the model. Optimization approaches are recently being developed to improve the maturity of *in-vitro* hiPSC-CMs and bring them closer to an adult phenotype.

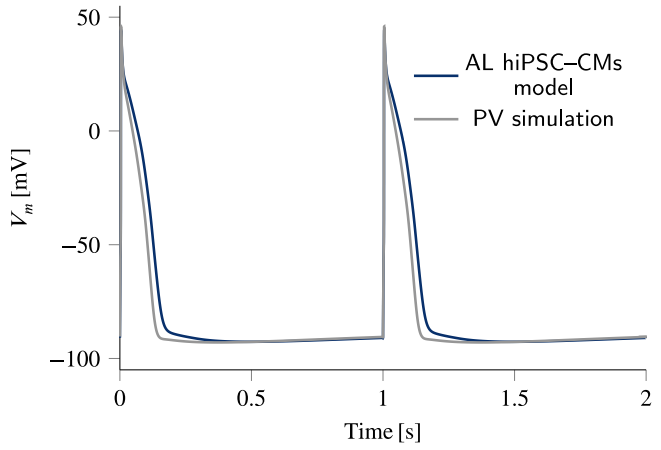

Fig. 9. PV simulation. Comparison between the simulated PV behaviour (grey line) and the presented AL hiPSC-CMs model (dark blue line) when considering the pacing at 1 Hz. The depicted figure highlights a shorter APD for PVs.

Nowadays, the challenge of hiPSC-CM maturation has been tackled *in-silico*, trying to provide more adult virtual models. In this direction, our novel AL hiPSC model provides a useful tool to quantitatively predict the impact of phenotype specific drugs.

Another limitation is the high variance of experimental data, while we have developed a model for the typical behaviour within a particular homogeneous population, averaging out the effects of inter-subject variation. In future work, we will consider to development a population of models in order to overcome the loss of information that cannot be considered when creating a new *in-silico* model.

Future perspectives absolutely consider the comparison with human adult models of atrial CMs and main differences with these models could suggest an operative direction towards the maturation of AL hiPSCs.

Finally, to reasonably simulate engineered tissue under pathological and non-basal conditions, the previously neglected atrial-specific currents $I_{K,ACh}$ and I_{K2P} will be included in the AL hiPSC-CMs model.

4.2. Future works

Future efforts to extend our study will take into account: (a) a different DC technique based on I_{Kur} instead of I_{K1} injection, using e.g. the Maleckar et al. [37] formulation (see Section 4); (b) the experimental investigation of the $I_{K,ACh}$ current in hiPSC-CMs and its incorporation into a modified version of our model; (c) the rate dependence of the I_{Kur} effects on AP repolarization in hiPSC-CMs; (d) the use of our model in large studies of *in-silico* populations to support the screening of different phenotype specific drug at various concentrations; (e) the spatio-temporal dynamic of hiPSC-CMs engineered tissues [48] by coupling the presented phenotype-specific ionic model with existing Monodomain or Bidomain reaction–diffusion electrophysiological models, which accurately integrate the space–time evolution of intracellular, extracellular and transmembrane potentials, [49]; (f) a mathematical approach to MEA field potential measurements for the analysis of drug effects on the electrical activity in order to facilitate a more comprehensive research and therapeutic development; (g) the study of patho-physiological arrhythmic events in regenerated cardiac tissues with chamber-specific ionic models.

5. Conclusion

In this study we have introduced a novel AL *in-silico* hiPSC-CMs model, based on a set of phenotype-specific membrane currents. This model is built on novel *in-vitro* experimental data just published in [1] to simulate the paced AP of matured AL hiPSC-CMs. The new model effectively recapitulates the electronic *in-vitro* hiPSC-CMs maturation process, transitioning from an unstable depolarized MDP to a hyperpolarized resting potential, and exhibits spontaneous firing activity in unpaced conditions. Finally, our model accurately reflects the experimental rate dependence data at CL $= 1000, 500, 250$ ms and demonstrates the expected response to the $4-$AP specific current blocker.

CRediT authorship contribution statement

Sofia Botti: Writing – review & editing, Writing – original draft, Methodology, Formal analysis. **Chiara Bartolucci:** Writing – review & editing, Formal analysis. **Claudia Altomare:** Writing – review & editing, Data curation. **Michelangelo Paci:** Methodology. **Lucio Barile:** Data curation, Conceptualization. **Rolf Krause:** Supervision, Conceptualization. **Luca Franco Pavarino:** Supervision, Conceptualization. **Stefano Severi:** Supervision, Methodology.

Declaration of competing interest

There are no conflicts of interest: None Declared.

Acknowledgements

This work was supported by the Swiss National Science Foundation under Grant numbers 217025 (S.B.); the Italian Ministry of University and Research under Grant PRIN PNRR 2022, P2002B38NR (L.F.P); and the European Union—NextGenerationEU through the Italian Ministry of University and Research under Grant PNRR—M4C2-I1.3, Project PR 00000019 “HEAL ITALIA” to S.S. CUP J33C22002920006 (C.B. and S.S.).

Code availability

The code of the AL hiPSC-CMs ionic model is public available on the GitHub repository at the following link
https://github.com/bottiso/AL_hiPSC_ionic model.git.

Supplementary Material

Appendix A. List of currents

This file contains the full list of membrane currents, exchanger and pumps, as well as the list of fluxes from the SR.

Appendix B. List of equations

This file contains the mathematical models, i.e. the full set of equations of our novel AL hiPSC ionic model and the list of constants and initial conditions at steady state. We highlighted in blue only the final changes in the VL hiPSC-CMs model [15].
Appendix A. List of the currents
This file contains the full list of membrane currents, exchanger and pumps, as well as the list of fluxes from the SR.

Appendix B: List of the equations
This file contains the mathematical models, i.e. the full set of equations of our novel AL hiPSC ionic model and the list of constants and initial conditions at steady state. We highlighted in blue only the final changes in the VL hiPSC-CMs model [15].

Appendix C. Supplementary data

Supplementary material related to this article can be found online at https://doi.org/10.1016/j.compbiomed.2024.108899.

References

[1] C. Altomare, C. Bartolucci, L. Sala, et al., A dynamic clamping approach using *in silico* IK1 current for discrimination of chamber-specific hiPSC-derived cardiomyocytes, Commun. Biol. 6 (1) (2023).

[2] K. Takahashi, S. Yamanaka, Induction of pluripotent stem cells from mouse embryonic and adult fibroblast cultures by defined factors, Cell 126 (4) (2006) 663–676.

[3] K. Takahashi, K. Tanabe, M. Ohnuki, M. Narita, T. Ichisaka, K. Tomoda, S. Yamanaka, Induction of pluripotent stem cells from adult human fibroblasts by defined factors, Cell 131 (5) (2007) 861–872.

[4] F.F. Darche, N.D. Ullrich, Z. Huang, M. Koenen, R. Rivinius, N. Frey, P.A. Schweizer, Improved generation of human induced pluripotent stem cell-derived cardiac pacemaker cells using novel differentiation protocols, Int. J. Mol. Sci. 23 (13) (2022).

[5] P. Pushp, D.E.S. Nogueira, C.A.V. Rodrigues, F.C. Ferreira, J.M.S. Cabral, M.K. Gupta, A concise review on induced pluripotent stem cell-derived cardiomyocytes for personalized regenerative medicine, Stem Cell Rev. Rep. 17 (3) (2021) 748—776.

[6] E.I. Parrotta, S. Scalise, L. Scaramuzzino, G. Cuda, Stem cells: The game changers of human cardiac disease modelling and regenerative medicine, Int. J. Mol. Sci. 20 (22) (2019).

[7] M. Vagos, I.G.M. van Herck, J. Sundnes, H.J. Arevalo, a.G. Edwards, J.T. Koivumäki, Computational modeling of electrophysiology and pharmacotherapy of atrial fibrillation: Recent advances and future challenges, Front. Physiol. 9 (2018).

[8] E. Wettwer, T. Christ, S. Endig, N. Rozmaritsa, K. Matschke, J.J. Lynch, M. Pourrier, J.K. Gibson, D. Fedida, M. Knaut, U. Ravens, The new antiarrhythmic drug vernakalant: ex vivo study of human atrial tissue from sinus rhythm and chronic atrial fibrillation, Cardiovasc. Res. 98 (1) (2013) 145–154.

[9] C. Yang, J. Al-Aama, M. Stojkovic, B. Keavney, a. Trafford, M. Lako, L. Armstrong, Concise review: Cardiac disease modeling using induced pluripotent stem cells, Stem Cells (Dayton, Ohio) 33 (9) (2015) 2643—2651.

[10] J. Li, Y. Hua, S. Miyagawa, J. Zhang, L. Li, L. Liu, Y. Sawa, Hipsc-derived cardiac tissue for disease modeling and drug discovery, Int. J. Mol. Sci. 21 (23) (2020).

[11] M. Paci, J. Hyttinen, K. Aalto-Setälä, S. Severi, Computational models of ventricular- and atrial-like human induced pluripotent stem cell derived cardiomyocytes, Ann. Biomed. Eng. 41 (11) (2013) 2334–2348.

[12] C.-A. Chapotte-Baldacci, M. Pierre, M. Djemai, M. Chahine, Characterizing ionic currents of atrial-like and ventricular-like hiPSC-cardiomyocytes, Biophys. J. 123 (3) (2024).

[13] H. Devalla, V. S., J. Ford, A. Verkerk, R. P., Atrial-like cardiomyocytes from human pluripotent stem cells are a robust preclinical model for assessing atrial-selective pharmacology, EMBO Mol. Med. 7 (4) (2015) 394–410.

[14] M. Casini, C. Fambuena Santos, R. Emig, R. Peyronnet, U. Ravens, I. Ontoria Oviedo, A. Climent, R. Sepulveda, In vitro model of atrial fibrillation: investigating the initiation and maintenance mechanisms of atrial remodeling using hiPSC-derived atrial cardiomyocytes, Eur. Heart J. 44 (Supplement_2) (2023) ehad655.3176.

[15] M. Paci, E. Passini, A. Klimas, S. Severi, et al., All-optical electrophysiology refines populations of in silico human iPSC-CMs for drug evaluation, Biophys. J. 118 (10) (2020) 2596–2611.

[16] M. Lemme, B.M. Ulmer, M.D. Lemoine, A.T. Zech, F. Flenner, U. Ravens, H. Reichenspurner, M. Rol-Garcia, G. Smith, A. Hansen, T. Christ, T. Eschenhagen, Atrial-like engineered heart tissue: An in vitro model of the human atrium, Stem Cell Rep. 11 (6) (2018) 1378–1390.

[17] C. Schulz, M. Sönmez, J. Krause, E. Schwedhelm, P. Bangfen, D. Alihodzic, A. Hansen, T. Eschenhagen, T. Christ, A critical role of retinoic acid concentration for the induction of a fully human-like atrial action potential phenotype in hiPSC-CM, Stem Cell Rep. (2023).

[18] D. Ismaili, C. Schulz, a. Horváth, J.T. Koivumäki, D. Mika, A. Hansen, T. Eschenhagen, T. Christ, Human induced pluripotent stem cell-derived cardiomyocytes as an electrophysiological model: Opportunities and challenges—The hamburg perspective, Front. Physiol. 14 (2023).

[19] J.T. Koivumäki, T. Korhonen, P. Tavi, Impact of sarcoplasmic reticulum calcium release on calcium dynamics and action potential morphology in human atrial myocytes: A computational study, PLoS Comp. Biol. 7 (2011) 1–14.

[20] P.H. Barry, J.W. Lynch, Liquid junction potentials and small cell effects in patch-clamp analysis, J. Membr. Biol. 121 (2) (1991) 101–117.

[21] M. Courtemanche, R. Ramirez, S. Nattel, Ionic mechanisms underlying human atrial action potential properties: Insights from a mathematical model, Amer. J. Physiol. 275 (1998) H301–21.

[22] L. Skibsbye, T. Jespersen, T. Christ, M. Maleckar, et al., Refractoriness in human atria: Time and voltage dependence of sodium channel availability, J. Mol. Cel. Card. 101 (2016).

[23] S. Botti, C. Bartolucci, C. Altomare, et al., Numerical simulations indicate IK1 dynamic clamp can unveil the phenotype of cardiomyocytes derived from induced pluripotent stem cells, in: Computing in Cardiology 2022, Vol. 49, 2022.

[24] A. Nygren, C. Fiset, L. Firek, J.W. Clark, et al., Mathematical model of an adult human atrial cell: the role of K+ currents in repolarization, Circ. Res. 82 1 (1998) 63–81.

[25] C. Bartolucci, M. Forouzandehmehr, S. Severi, M. Paci, A novel in silico electromechanical model of human ventricular cardiomyocyte, Front. Physiol. 13 (2022).

[26] K.H. Jæger, V. Charwat, S. Wall, K.E. Healy, A. Tveito, Identifying drug response by combining measurements of the membrane potential, the cytosolic calcium concentration, and the extracellular potential in microphysiological systems, Front. Pharmacol. 11 (2021).

[27] E. Wettwer, O. Hála, T. Christ, J.F. Heubach, D. Dobrev, M. Knaut, A. Varró, U. Ravens, Role of IKur in controlling action potential shape and contractility in the human atrium, Circulation 110 (16) (2004) 2299–2306.

[28] Z. Wang, B. Fermini, S. Nattel, Sustained depolarization-induced outward current in human atrial myocytes. Evidence for a novel delayed rectifier K+ current similar to Kv1.5 cloned channel currents, Circ. Res. 73 (6) (1993) 1061–1076.

[29] K.H. Jæger, S. Wall, A. Tveito, Computational prediction of drug response in short QT syndrome type 1 based on measurements of compound effect in stem cell-derived cardiomyocytes, PLoS Comput. Biol. 17 (2) (2021) 1–32.

[30] K.H. Jæger, A.G. Edwards, W.R. Giles, A. Tveito, A computational method for identifying an optimal combination of existing drugs to repair the action potentials of SQT1 ventricular myocytes, PLoS Comput. Biol. 17 (8) (2021) 1–24.

[31] J.T. Koivumäki, N. Naumenko, T. Tuomainen, J. Takalo, et al., Structural immaturity of human iPSC-derived cardiomyocytes: In silico investigation of effects on function and disease modeling, Front. Physiol. 9 (2018).

[32] D.C. Kernik, S. Morotti, H. Wu, P. Garg, et al., A computational model of induced pluripotent stem-cell derived cardiomyocytes incorporating experimental variability from multiple data sources, J. Physiol. 597 (17) (2019) 4533–4564.

[33] M. Paci, J. Koivumäki, H. Lu, D. Gallacher, et al., Comparison of the simulated response of three in silico human stem cell-derived cardiomyocytes models and in vitro data under 15 drug actions, Front. Pharmacol. 12 (2021).

[34] M. Vagos, I.G.M. van Herck, J. Sundnes, H.J. Arevalo, A.G. Edwards, J.T. Koivumäki, Computational modeling of electrophysiology and pharmacotherapy of atrial fibrillation: Recent advances and future challenges, Front. Physiol. 9 (2018).

[35] S. Hilderink, H.D. Devalla, L. Bosch, R. Wilders, A.O. Verkerk, Ultrarapid delayed rectifier K+ channelopathies in human induced pluripotent stem cell-derived cardiomyocytes, Front. Cell Dev. Biol. 8 (2020).

[36] A.O. Verkerk, R. Wilders, Injection of IK1 through dynamic clamp can make all the difference in patch-clamp studies on hipsc-derived cardiomyocytes, Front. Physiol. 14 (2023).

[37] M.M. Maleckar, J.L. Greenstein, W.R. Giles, N.A. Trayanova, K+ current changes account for the rate dependence of the action potential in the human atrial myocyte, Am. J. Physiol.-Heart Circ. Physiol. 297 (4) (2009) H1398–H1410.

[38] V.A. Maltsev, E.G. Lakatta, A novel quantitative explanation for the autonomic modulation of cardiac pacemaker cell automaticity via a dynamic system of sarcolemmal and intracellular proteins, Am. J. Physiol.-Heart Circ. Physiol. 298 (6) (2010) H2010–H2023.

[39] E. Grandi, S.V. Pandit, N. Voigt, A.J. Workman, D. Dobrev, J. Jalife, D.M. Bers, Human atrial action potential and Ca^{2+} model, Circ. Res. 109 (9) (2011) 1055–1066.

[40] C. Schmidt, F. Wiedmann, N. Voigt, et al., Upregulation of K(2P)3.1 K+ current causes action potential shortening in patients with chronic atrial fibrillation, Circulation 132 (2015).

[41] M. Paci, S. Casini, M. Bellin, J. Hyttinen, S. Severi, Large-scale simulation of the phenotypical variability induced by loss-of-function long QT mutations in human induced pluripotent stem cell cardiomyocytes, Int. J. Mol. Sci. 19 (11) (2018).

[42] M. Paci, E. Passini, S. Severi, J. Hyttinen, B. Rodriguez, Phenotypic variability in LQT3 human induced pluripotent stem cell-derived cardiomyocytes and their response to antiarrhythmic pharmacologic therapy: An in silico approach, Heart Rhythm 14 (11) (2017) 1704–1712.

[43] O.J. Britton, A. Bueno-Orovio, K.V. Ammel, H.R. Lu, R. Towart, D.J. Gallacher, B. Rodriguez, Experimentally calibrated population of models predicts and explains intersubject variability in cardiac cellular electrophysiology, Proc. Natl. Acad. Sci. 110 (23) (2013) E2098–E2105.

[44] P. Melnyk, J.R. Ehrlich, M. Pourrier, L. Villeneuve, T.-J. Cha, S. Nattel, Comparison of ion channel distribution and expression in cardiomyocytes of canine pulmonary veins versus left atrium, Cardiovasc. Res. 65 (1) (2005) 104–116.

[45] E. Abbate, M. Boulakia, Y. Coudière, J.-F. Gerbeau, P. Zitoun, N. Zemzemi, In silico assessment of the effects of various compounds in MEA/hiPSC-CM assays: Modeling and numerical simulations, J. Pharmacol. Toxicol. Methods 89 (2018) 59–72.

[46] A.O. Verkerk, R. Wilders, Dynamic clamp in electrophysiological studies on stem cell–derived cardiomyocytes—Why and how? J. Cardiovasc. Pharmacol. 77 (3) (2021).

[47] A.O. Verkerk, C.C. Veerman, J.G. Zegers, I. Mengarelli, C.R. Bezzina, R. Wilders, Patch-clamp recording from human induced pluripotent stem cell-derived cardiomyocytes: Improving action potential characteristics through dynamic clamp, J. Mol. Sci. 18 (9) (2017).

[48] S. Botti, M. Torre, Isogeometric simulation of a derived stem cell engineered ventricle, Adv. Comput. Sci. Eng. 1 (3) (2023) 298–319.

[49] P.C. Franzone, L.F. Pavarino, S. Scacchi, Mathematical Cardiac Electrophysiology, vol. 13, Springer, 2014.